On Force-Displacement Characteristics and Surface Deformation in Piezo Vibration Striking Treatment (PVST)

Jisheng Chen, Yang Xu, Juan Sandoval, Patrick Kwon, Yang Guo[1]

Department of Mechanical Engineering, Michigan State University, East Lansing, MI 48824

Abstract: This paper presents an experimental study on a novel mechanical surface treatment process, namely piezo vibration striking treatment (PVST), which is realized by a piezo stack vibration device installed on a CNC machine. Unlike other striking-based surface treatments, PVST employs non-resonant mode piezo vibration to induce controllable tool strikes on workpiece surface. In this study, an experimental setup of PVST is implemented. Four types of experiments, i.e., tool-surface approaching, single-spot striking, 1D scan striking, and 2D scan striking, are conducted to investigate the relationships among the striking force, tool vibration displacement, and surface deformation in PVST. The study shows that PVST can induce strikes with consistent intensity in each cycle of tool vibration. Both the striking intensity and striking location can be well controlled. Such process capability is particularly demonstrated by the resulting texture and roughness of the treated surfaces. Moreover, two linear force relationships have been found in PVST. The first linear relationship is between the striking force and the reduction in vibration amplitude during striking. The second one is between the striking force and the permanent indentation depth created by the strike. These linear force relationships offer the opportunity to realize real-time monitoring and force-based feedback control of PVST. This study is the first step towards developing PVST as a more efficient deformation-based surface modification process.

Keywords: surface treatment; peening; plastic deformation; indentation; surface texture

[1] Corresponding author. Email: yguo@msu.edu.

INTRODUCTION

Because friction, wear, corrosion, and fatigue usually intensify on the surface, the performance and service life of engineering components are strongly dependent on their surface attributes, such as surface roughness, hardness, microstructure, and residual stress [1]. Modifying these surface attributes is an effective and economical way of improving the overall performance of engineering components and products.

A common method to modify surface attributes is by surface plastic deformation imposed by striking the surface with hard tool indenters. The most notable example is shot peening (SP) [2,3]. In SP, a myriad of small hard balls made of steel or ceramic is impacted onto the surface by compressed air, resulting in randomly distributed strikes on the targeted surface. The process will generate compressive residual stresses on the surface and thereby improve the fatigue strength of critical components and the overall fatigue life of a structure [4,5]. Surface mechanical attrition treatment (SMAT) is another striking-based surface modification process [6]. In SMAT, hard steel balls (used as tool indenters) and the workpiece are all confined inside a vibrating chamber. The workpiece is fixed with the chamber while the steel balls are free to bounce between the workpiece surface and the chamber walls, leading to repeated strikes on the workpiece surface. This process emphasizes on inducing severe plastic deformation which transforms the surfaces into a nanocrystalline microstructure [7,8]. In both SP and SMAT, the surface is struck by numerous free indenters whose kinematics are not directly controlled. The striking location, striking angle, and striking force associated with each indenter are random variables in a large extent. The accumulated effect from these strikes is therefore of stochastic nature, which makes it difficult to control the treatment quantitatively. In addition, since the

exact locations of these random strikes cannot be strictly controlled, these processes suffer from poor reliability.

Alternatively, surface striking can be also realized while controlling the striking location by a single vibrating tool indenter(s) driven by either a pneumatic or ultrasonic actuator. This is demonstrated by high frequency mechanical impact (HFMI) treatment which is mainly used to treat weld joints [9]. The HFMI equipment is usually made as a hand-held impact device connecting to an external power source, which enables the treatment to be carried out manually for weldments of large sizes or complex geometries. The impact device is usually directed to strike the weld toe to modify its geometry, induce compressive residual stress, and close subsurface micro-cracks, which can significantly enhance the fatigue strength of the weld joints [10,11]. Although it is possible to treat the weld joints manually with a hand-held equipment, the manual operation is apparently not ideal for treating component surfaces generally. Machine hammer peening (MHP) treatment [12,13] and ultrasonic nanocrystal surface modification (UNSM) treatment [14,15] are the examples of such devices integrated onto a CNC machine or robotic arm. MHP has been shown to be effective for reducing surface roughness and increasing surface hardness for machined molds and dies [16,17]. As indicated by its name, UNSM employs ultrasonic tool vibration which enables generating nanocrystalline surfaces and improving tribological and fatigue properties [14,18]. From the process control point of view, the main advantage of MHP and UNSM is that the scanning path of the vibrating tool over the surface can be precisely controlled by the CNC machine, which implies that the strikes on the surface can be much better controlled compared to SP, SMAT, and HFMI.

While a CNC machine enables more precise positioning of the strikes, the control of each strike still depends on the striking device. In MHP, the striking device can be pneumatically or ultrasonically driven [10,13,19]. The indenter held in the front of the device is usually not rigidly connected to the actuator. While the actuator repeatedly impacts the indenter, the relative motion between indenter and actuator cannot be strictly controlled. Therefore, the impact on the surface may be only energy controlled similar to SP but cannot be delivered in consistent intensity [20]. In UNSM, the motion of the indenter is fully driven by the rigidly connected ultrasonic actuator, leading to more uniform strikes on the surface [14]. However, ultrasonic vibration depends on the resonance of the vibrating structure and thus its frequency and amplitude cannot be controlled [21]. Technically, the vibration displacement and the striking force are difficult to measure in the ultrasonic frequency regime. This makes it difficult to monitor or control surface deformation imposed by each individual strike, and the overall surface deformation resulting from the treatment then cannot be quantitatively controlled. Note that imposing controllable surface deformation is a critical step towards understanding and controlling the modified surface attributes [22].

Comparing with ultrasonic vibration, the non-resonant vibration directly driven by piezo stack actuation is more convenient to control. This has been demonstrated in its applications in vibration assisted turning and drilling processes [23–25]. The non-resonant piezo vibration often has a lower vibration frequency but can achieve a higher vibration amplitude (up to 200 µm stroke piezo stack is commercially available). The frequency and amplitude can be independently controlled with the piezo stack actuation. Monitoring the vibration displacement and striking

force within each vibration cycle also becomes possible. These characteristics make non-resonant piezo vibration more suitable for imposing controlled strikes and deformation on the surface.

In this study, a vibration striking device enabled by non-resonant mode piezo stack actuation is developed. Using this device integrated into a CNC machine, piezo vibration striking experiments are conducted to investigate the striking force, tool vibration displacement, and the resulting surface deformation. The study reveals the feasibility and the promising capability of piezo vibration striking treatment (PVST) in inducing controllable surface plastic deformation. This is the first step towards developing PVST as a more efficient process for enabling deformation-based surface modification including finish, residual stress, hardness, microstructure, and hence enhancing components' performance such as fatigue life and wear resistance.

EXPERIMENTAL SETUP

Figure 1 shows the experimental setup of PVST. The developed piezo vibration striking device (Fig. 1b) is mounted onto the spindle of a CNC vertical milling machine (Hass VF-4) through a standard CAT 40 tool holder. The spindle rotation function in the machine is locked to provide only the vertical motion of the striking device along the Z axis, which is capable to control the striking distance between striking tool and workpiece surface. The workpiece is mounted on the machine table which provides the horizontal motion of the workpiece in both X and Y axes for the striking location.

The piezo vibration striking device is realized using non-resonant mode piezo stack actuation. Figure 1c shows the schematic of the striking device assembly. Inside the device body,

a piezo stack actuator is assembled with a spline shaft along the axial direction. The piezo stack is compressed by the shaft through an internal pre-loaded spring. A ball spline bearing is mounted on the spline shaft and fixed with the device body, which allows the linear motion of the shaft in the axial direction while restricting the bending and rotation of the shaft. The striking tool indenter, in the form of a small cylinder with a hemispherical end, is rigidly connected to the end of the shaft. The tool indenter is made of M2 high speed steel with the diameter of 3 mm. The vibration of the indenter is actuated by the extension and contraction of the piezo stack which is controlled by the driving voltage from a waveform generator and a power amplifier.

To monitor the striking process, the vibration displacement of the indenter tool is measured using a capacitance displacement probe (Capacitec HPC-40). As shown in Fig. 1b and 1c, the probe is clamped on the device body and facing the flat surface of a flange that is part of the vibrating shaft. The displacement is measured based on the change in the gap between the probe and the flange. The striking force is measured using a dynamometer plate (Kistler 9527B) on the workpiece mounted on the CNC machine table. The measured displacement and force signals are recorded using a data acquisition system (NI USB 6361 + LabView). The sampling rate for both signals is 4000 per second which is at least 40 times higher than the tool vibration frequencies used in the study; therefore, the displacement and force signals during each vibration or striking cycle can be sufficiently captured.

The frequency and amplitude of tool vibration are controlled by varying the frequency and amplitude of the sinusoidal driving voltage. The lower bound of the driving voltage is always set at zero and thus the upper bound of the driving voltage is equal to the peak-to-peak amplitude (V_{pp}) of the voltage oscillation. The maximum driving voltage allowed for the piezo stack is 150 V.

The nominal stroke of the piezo stack is 100 µm. Figure 2 shows the calibrated tool vibration of the device assembly without any load at the driving voltage frequency (f) of 10 and 100 Hz and the driving voltage amplitude (V_{pp}) of 60, 90, 120 and 150 V. Fig. 2a shows that the vibration displacement of the tool (u) closely follows the sinusoidal driving voltage (V). The tool vibration frequency is the same as the driving voltage frequency. The tool vibration amplitude without striking (u^0_{pp}) is proportional to the driving voltage amplitude (V_{pp}) and is not significantly affected by the vibration frequency (Fig. 2b). The maximum vibration amplitude achieved at V_{pp} = 150 V is about 90 µm, which is 10% lower than the nominal stroke (100 µm). The calibration results indicate the frequency and amplitude of tool vibration can be conveniently and independently controlled. Note that the driving voltage conditions calibrated here are used to conduct the vibration striking experiments in this study.

Figure 3 gives an overview of the four basic experiments conducted in this study. The first experiment (Fig. 3a) investigates the tool-surface approaching process in which the vibrating tool is fed vertically towards the workpiece surface. The second experiment (Fig. 3b) investigates the single spot striking process in which the vibrating tool repeatedly strikes the same location on the workpiece surface from a fixed tool vertical position. The third experiment (Fig. 3c) investigates the 1D scan vibration striking process in which the vibrating tool strikes the workpiece surface while it is continuously moving along a linear path. We will refer the horizontal tool feed motion as the tool scan motion in this study. The fourth experiment (Fig. 3d) investigates the 2D scan vibration striking process which is the extension of the 1D scan striking to treat a 2D surface area using the vibrating tool with parallel scan path lines. These experiments are designed for better understanding the relationships among tool displacement, striking force,

and surface deformation in non-resonant vibration striking surface treatment enabled by piezo stack actuation.

For all experiments, the workpiece material is mild steel ASTM A572GR50 with a dimension of 120mm × 40mm × 20mm. The initial surface of the workpiece is prepared by grinding to have the roughness (Sa) of 0.32 μm. Note that the uniform initial smooth surface is necessary to characterize and understand the deformed surface resulting from the striking. 3D surface profiles are characterized using Keyence Digital Microscope.

RESULTS

Tool-Surface Approaching

In the tool-surface approaching experiment (Fig. 3a), the initial vertical (Z) position of the tool is set to 120 μm, i.e., Z = 120 μm with the reference from the workpiece surface. The vibration of the tool is turned on and fed onto the surface at a speed of 1 μm/s. Figure 4 shows the measured force (F) and tool vibration displacement (u) plotted against the tool position (Z) as the vibrating tool is fed towards the workpiece at f = 100 Hz and V_{pp} = 150 V. Note u refers to the displacement of the vibrating tool while Z refers to the tool position during the feed motion. In the regime A of the tool position (from Z = 120 μm to Z = 105 μm), the tool has no contact with the workpiece surface without any load on the vibrating tool. The vibration of the tool has the constant and calibrated amplitude. Entering the regime B (from Z = 105 μm to Z = -55 μm), the vibrating tool begins to engage and disengage the workpiece in each vibration cycle during the repeated strikes on the surface. The peak force of each successive strike increases steadily because the indentation depth reached by each successive strike increases as the tool position Z decreases. At the same time, the reduction in the vibration displacement of the tool is evident

due to the elastic compression of the vibration device by the striking force. The higher the striking force, the lower the vibration displacement. Therefore, the maximum displacement of the tool in each successive vibration cycle (or striking cycle) decreases steadily with the tool position Z. However, the minimum displacement of the tool remains unchanged when the tool disengaged and hence no force to compress the piezo stack. Entering the regime C ($Z < -50$ µm), the vibrating tool becomes continuously engaged with the workpiece during its vibration. As a result, the force in each vibration cycle increases steadily with the decrease of tool position Z. Correspondingly, the vibration displacement of the tool also decreases with the tool position Z.

In the approaching experiment, the vibration striking occurs in the regime B which includes the tool position both above ($Z > 0$) and below ($Z < 0$) the initial workpiece surface. For practical application of vibration striking treatment, the vibrating tool also needs to move horizontally (in the X – Y plane) in order to impose the strike at any location on the surface. When considering the horizontal tool motion, the tool vertical position below the initial surface ($Z < 0$) will result in the continuous engagement between the tool and the workpiece, which will generate significant sliding-type deformation on the surface. To minimize the sliding deformation, the tool position for inducing vibration striking should be limited to $Z \geq 0$. The upper bound of the tool position is equal to the maximum vibration displacement under no load condition (u^0_{max}) since no contact occurs when $Z > u^0_{max}$.

As noted already, the maximum vibration displacement (u_{max}) during the striking process is dependent on the striking force. Figures 5a and b show the relationship between the reduction in maximum vibration displacement ($\Delta u_{max} = u^0_{max} - u_{max}$) and the peak force of the strike (F_{max}) at f = 10 and 100 Hz, respectively. The relationship is based on the force and displacement data

corresponding to the tool position range $0 < Z < u^0_{max}$ in the approaching experiment. Note in this Z range, the reduction in maximum vibration displacement is the same as the reduction in vibration amplitude ($\Delta u_{pp} = u^0_{pp} - u_{pp}$). The relationship between F_{max} and Δu_{max} (or Δu_{pp}) is clearly linear, which gives a stiffness value of 11.1 N/μm at f = 10 Hz (Fig. 5a) and 11.4 N/μm at f = 100 Hz (Fig. 5b). The axial stiffness of the vibration device assembly is nearly identical at 11.7 N/μm (Fig. 5c) confirmed by a static compression test on the device (with no vibration). Therefore, the reduction in vibration displacement is due to the elastic compression of the device assembly under the striking force, which means the reduction in vibration displacement can be calculated from the force signal given the stiffness of the vibration device.

Single Spot Vibration Striking

The single spot vibration striking experiment (Fig. 3b) is conducted on a single surface spot with a fixed tool position Z = 0. With the initial tool position Z set to zero, the vibration is turned on for a duration of 3 seconds to induce repeated strikes on the same surface spot. It is expected the plastic deformation is imposed only within the first few strikes. After reaching a steady state, the repeated strikes only involve elastic deformation of the deformed surface. This is confirmed by Fig. 6 which shows the measured force and vibration displacement during the repeated strikes at the vibration condition f = 10 Hz and V_{pp} = 150 V. It is observed both the force and displacement signals reach the steady-state oscillations nearly right after the starting of the tool vibration. The peak force (F_{max}) and the maximum vibration displacement (u_{max}) then remain constant. For other vibration conditions, the measured force and vibration displacement signals show similar steady state oscillations except that F_{max} and u_{max} are different. Figure 7 summarizes the measured F_{max} and u_{max} at various vibration conditions (V_{pp} = 60, 90, 120, 150 V, f = 10 and

100 Hz). It is observed that both F_{max} and u_{max} increase with V_{pp} which is expected since higher V_{pp} means higher vibration amplitude. It is also observed that higher f results in higher F_{max} but lower u_{max} for a given V_{pp}. The higher F_{max} may be partially attributed to the increased inertial force which the tool needs to overcome to accelerate the workpiece material when it strikes the surface. Higher frequency leads to higher acceleration during each strike and hence higher striking force. The lower u_{max} is consistent with the higher F_{max} since there is more reduction in vibration displacement due to the elastic compression of the vibration device (see Fig. 5).

Figure 8a shows the resulting permanent indentation on the surface at each vibration condition. Figures 8b and c show the cross-sectional profiles of these indentations grouped at f = 10 and 100 Hz, respectively. It is observed that the depth (h) and diameter (D) of the indentation increase with V_{pp}. For a given V_{pp}, higher f results in higher h and D. As noted earlier, a higher f results in a lower u_{max} (Fig. 7b). Since the tool position is at Z = 0, u_{max} is equal to the maximum indentation depth reached by the strike, which represents the total plastic and elastic deformation. In contrast, h represents only the plastic deformation. Then it can be deduced that a higher f leads to a larger plastic deformation (Fig. 7c) despite of a smaller total deformation (Fig.7b). The higher plastic deformation leads to more strain hardening of the material which can also contribute to the higher F_{max} for higher f (see Fig. 7a). It should be noted the comparison of F_{max} is at the steady state striking stage where the plastic deformation has already completed and only elastic deformation is taking place, so the observed difference in F_{max} for different f is not attributed to the strain rate effect which occurs only during plastic deformation.

Figure 9 shows how F_{max} is related with h and D, respectively. It is found that the size of the permanent indentation generated on the surface is linearly dependent on the peak force of

the strike. This indicates the force signal can be used to monitor the plastic deformation imposed by each strike.

1D Scan Vibration Striking

In this experiment (Fig. 3c), after the tool position in Z is set to zero (Z = 0), tool vibration is turned on, and the workpiece is moved horizontally along the X axis at a controlled speed (v_s). This leads to the vibrating tool scanning the surface while imposing successive strikes along a straight tool path. The offset distance (d_s) between two successive strikes is dependent on the vibration frequency (f) and the scan speed (v_s) as

$$d_s = v_s / f \qquad (1)$$

Figure 10 shows the surface grooves created with the vibration condition f = 100 Hz and V_{pp} = 150 V at four scan speeds v_s = 3300, 2475, 1650, 825 mm/min. These scan speeds are selected to achieve the striking overlap ratios of 0, 0.25, 0.5, and 0.75, respectively. The overlap ratio (r_o) is defined as (Fig. 10a)

$$r_o = (D - d_s) / D \qquad (2)$$

where D is the indentation diameter obtained from the single spot vibration striking experiment (see Fig. 8). According to Eqs. 1 and 2, a lower v_s leads to a smaller d_s and thus a higher r_o. Figure 10b and c show that the 1D scan vibration striking results in uniform indentation pattern along the tool path at each scan speed. The higher the r_o, the smoother the surface in the groove.

Figure 11a shows the longitudinal section profiles of these grooves. The indentation spacing d_s can be measured from these profiles as 516 ± 8, 392 ± 12, 269 ± 13 and 131 ± 8 μm for r_o = 0, 0.25, 0.5, and 0.75, respectively. The measured d_s's agree well with the calculated d_s's using Eq.

1. This indicates the vibration striking with tool scan motion can be accurately controlled. Furthermore, the measured peak-to-valley height (R_z) for the longitudinal section profiles are 17.0, 10.5, 7.6, and 1.6 μm, respectively, which indicates again higher r_o leads to smoother surface in the groove.

Figure 11b shows the transverse section profiles of these grooves (perpendicular to the tool scan direction) taken at the center of each indentation which corresponds to the maximum depth location in the groove. As readily observed, the transverse section profile is not much affected by r_o. The profile appears nearly the same for different r_o. The groove depth (h) measured from the undeformed surface is about 24 μm. The groove width measured by the distance between the two ridges is about 645 μm. The two ridges are formed by displacing material within the groove. The ridge size increases slightly with r_o as more material tends to be displaced, which also creates smoother surface in the groove. Note the left ridge is slightly higher than the right ridge for all cases, which is likely caused by imperfect mounting of the workpiece in the experiment that results in slight tilting of the initial surface.

Figure 12 shows the measured forces corresponding to these grooves. There are two force components during 1D scan vibration striking: the striking force (F_z) in the Z direction and the sliding force (F_x) in the X direction. Both forces are highly repetitive in the successive striking cycles, which indicates the process is quite stable. The primary force is the striking force which is not significantly affected by r_o. The peak of the striking force is around 550 N for all cases. The secondary force is the sliding force which is much smaller than the striking force. The sliding force is generated due to the horizontal scan motion of the tool. Unlike the striking force, which has symmetrical profile and nearly independent of r_o, the sliding force decreases with increasing r_o,

and the force profile also becomes more asymmetrical. The asymmetrical profile indicates the sliding force increases even when the tool is pulling from the surface after it reaches the maximum vibration displacement. This is likely caused by the generation of pile-up material in front of the tool due to sliding. The sliding force is dependent on the effective engagement depth between the tool and workpiece surface during sliding. Besides the tool vibration displacement, the effective engagement depth is also affected by the amount of pile-up material in front of the tool. While the tool is retracting from its maximum vibration displacement which tends to reduce the effective engagement depth, the continuous sliding action keeps generating pile-up material in front of the tool which tends to increase the effective engagement depth. As a result, the occurrence of the maximum engagement depth (corresponding to the sliding force peak) lags the maximum vibration displacement (corresponding to the striking force peak) which then results in the asymmetrical profile of the sliding force.

Besides varying r_o, the 1D scan vibration striking experiment has also been conducted while varying V_{pp}. Figure 13 summarizes the measured groove depth (h) and width (W) for all cases. It shows that the groove depth and width are primarily dependent on V_{pp} (i.e., vibration amplitude) and less on r_o. Moreover, it is found again the depth and width of the groove are linearly dependent on the striking peak force (Fig. 14) despite the difference in the slope from the single spot vibration striking experiment (see Fig. 9). Therefore, the indentation deformation resulting from each individual strike with tool scan motion can be also monitored using the force signal.

2D Scan Vibration Striking

In this experiment, a 5 mm x 5 mm area of the workpiece surface is treated by the vibrating tool following parallel line scan paths. For all cases, the spacing (d_p) between the path lines is set

to be the same as the offset distance (d_s) between two successive striking locations along the scan path (see Fig. 15a). This results in approximately the same striking overlap ratio r_o in both the scan direction and the transverse direction with respect to the scan path lines. The effects of V_{pp} and r_o on the topography of the treated surface are investigated.

Figure 15 shows the surface topography obtained at various V_{pp} and r_o. The upper row is for different r_o (0, 0.25, 0.5 and 0.75) with fixed V_{pp} (120 V) while the lower row is for different V_{pp} (60, 90, 120, and 150 V) with fixed r_o (0.75). For each condition, the generated surface texture is uniform throughout the treated area, which reflects the uniform spacing and intensity of the strikes during the treatment. The r_o significantly affects the generated surface texture. With the small r_o (Fig. 15a and 15b), the surfaces have a dimple texture that reflects each indentation on the surface. It shows that the material is displaced to form circular ridges. However, more material is displaced to the two lateral sides compared to the front and back sides with respect to the tool scan path. As r_o increases, the dimple size decreases. When r_o is increased to 0.75, individual dimple is no longer visible (Fig. 15d). When the surfaces generated at r_o = 0.75 are examined at a higher resolution (Fig. 15e-h), line ridges parallel to the tool scan path can be observed on the surfaces at higher V_{pp}. These line ridges are formed mainly by the lateral displacement of the material from inside the tool paths. The height of these line ridges decreases with decreasing V_{pp}. At r_o = 0.75 and V_{pp} = 60 V (Fig. 15e), the line ridges are no longer visible. The surface texture appears to have no significant difference along the scan direction and its transverse direction, leading to a more isotropic texture.

Figure 16 summarizes the quantified roughness parameters (S_a, R_a, and R_z) for these surfaces. The 1D roughness parameters R_a and R_z are measured along both the scan and the transverse

directions. It shows that all roughness parameters decrease with the increase in r_o and decrease in V_{pp}. For $r_o < 0.75$, R_a and R_z are significantly higher in the transverse direction than the scan direction, and S_a is very close to the R_a in the scan direction (Fig. 16a and 16b). For $r_o = 0.75$, the roughness difference in the two directions is significantly reduced, and the difference is further reduced with decreasing V_{pp} (Fig. 16c and 16d). These changes are consistent with the transition of surface texture from the dimple type to the line type and eventually to the isotropic type.

Note the roughness of the treated surfaces is all higher than the initial roughness for the ground surface. The smoothly ground surface was used to minimize the influence of initial surface roughness and texture such that the generated surface roughness and texture can be easily related to the processing parameters of the vibration striking treatment. Furthermore, these measured roughness parameters represent the achievable surface roughness using the corresponding treatment parameters. Among all the surfaces shown in Fig. 15, the smoothest surface is obtained with $V_{pp} = 60$ V and $r_o = 0.75$ at $S_a = 0.44$ μm, which is only slightly higher than the initial S_a value of 0.32 μm for the ground surface.

DISCUSSIONS

The results from the four experiments demonstrate the feasibility and excellent controllability of piezo vibration striking treatment (PVST) in terms of force and vibration displacement monitoring and surface deformation control. The important process parameters for PVST are tool vertical position in Z, tool vibration frequency f and amplitude u_{pp}, striking overlap ratio r_o, and tool scan path. By combining piezo stack actuated vibration device with CNC machine, these process parameters can be directly or indirectly controlled as well as monitored in real time. In general, the piezo stack vibration device enables the control of tool vibration

frequency and amplitude while the CNC machine enables the control of tool position in Z and tool scan motion (speed and path). The control of tool vibration and tool vertical position is critical for controlling the local surface deformation imposed by each individual strike while the control of tool scan motion is critical for controlling the locations and layout of the successive strikes. Such combined process controllability will lead to enhanced controllable surface deformation which is beyond the capability of current striking-based treatment processes, such as SP, SMAT, MHP, and UNSM. Therefore, PVST has the potential to realize more efficient deformation-based surface engineering including finish, residual stress, hardness, and microstructure for enhancing components' performance such as fatigue life and wear resistance.

The 2D vibration striking experiment has shown surface finish can be improved by increasing r_o and/or decreasing $V_{pp.}$ The trade-offs in different combinations of r_o and V_{pp} which can achieve the same level of surface finish are worth further discussion. In general, the same level of surface finish may be achieved by the combination of higher r_o and higher V_{pp} or the combination of lower r_o and lower V_{pp}. Higher r_o can be achieved by reducing the tool scan speed which will increase the treatment time. It can be also achieved by increasing tool vibration frequency which will increase the power consumption for piezo stack actuation. Higher V_{pp} leads to higher plastic strain and thicker deformed layer due to higher vibration amplitude. In contrast, the combination of lower r_o and lower V_{pp} results in faster treatment and less vibration power consumption. However, the induced plastic strain and strained layer thickness is smaller. Based on these trade-offs, the higher r_o – higher V_{pp} setting is more suitable for surface microstructure refinement purpose while the lower r_o – lower V_{pp} setting is more suitable for surface residual stress modification purpose.

Both the striking force and tool vibration displacement in PVST can be directly measured in real time. This is a major advantage over the ultrasonic vibration surface treatment, for it offers an opportunity for realizing real-time monitoring and control of the treatment process. Two linear force relationships which are found in PVST are particularly useful in this regard. The first linear relationship is between the striking force and the reduction in tool vibration amplitude shown in Fig. 5. The amplitude reduction is due to the elastic deformation of the device assembly under the striking force. This linear relationship reflects the stiffness of the device assembly and is independent of workpiece material and striking tip geometry. It can be used to calculate the vibration amplitude during striking from the force signal:

$$u_{pp} = u_{pp}^{0} - \Delta u_{pp} = m * V_{pp} - F_{max} / K \qquad (3)$$

where m is the proportionality between the unloaded vibration amplitude and the input driving voltage; K is the proportionality between the striking peak force and the reduction in vibration amplitude which is equivalent to the stiffness of the device assembly. Both m and K are the characteristics of the piezo vibration device and can be obtained by device calibration as shown in Fig. 2c and Fig. 5. Since V_{pp} is a directly controlled input parameter and F_{max} can be obtained from the measured force signal, it is then possible, based on Eq. 3, to monitor the vibration amplitude in PVST without directly measuring the vibration displacement but instead using the measured force signal. This will simplify the instrumentation for process monitoring.

The second linear force relationship is found between the striking force and the resulting indentation size (Figs. 9 and 14). This relationship should depend on the workpiece material and the striking tool tip geometry since both affect the plastic deformation induced on the surface.

For the workpiece material (mild steel) and striking tip (d=3mm) used in this study, the force – indentation size relationship can be well approximated as being linear. Theoretically, this relationship is nonlinear for a spherical shaped indenter [26]. However, the indentation depth range of PVST is usually very small (e.g., ~ 30μm in Figs. 9 and 14) compared to the striking tool tip diameter (3mm). It is this small indentation depth range that enables the good approximation of the linear relationship between the striking force and indentation size. The quality of this linear approximation can be considered to depend on the ratio of the indentation depth range to the diameter of the striking tool tip (h/D). The smaller this ratio, the better quality has the linear approximation. It can be expected that the linear force relationship is better approximated for a harder material than for a softer material because h becomes smaller for the harder material and better for a larger striking tool tip than for a smaller tool tip.

In practice, the h/D ratio may still be very small despite the changes of workpiece material or tool tip size, so the linear force – indentation size relationship may be broadly acceptable in PVST. The linear equation describing the relationship, however, will change with the workpiece material and the striking tool tip diameter. For a given combination of workpiece material and tool tip diameter, the linear force – indentation size relationship should be fixed, based on which the indentation size or plastic deformation level induced by each individual strike can be monitored using the measured force signal.

The two linear force relationships provide a basis for realizing real-time monitoring and force-based feedback control of PVST which can greatly enhance the treatment efficiency and capability. For practical implementation, the force sensor eventually needs to be integrated in the vibration device. This type of integration has been demonstrated feasible although for

implementation of modulation-assisted drilling process [23,24]. In this study, PVST is only performed on a flat workpiece surface. The force-based feedback control capability will be very useful for performing the treatment on a freeform surface. In this case, the tool vertical position and vibration amplitude can be controlled in real time based on the striking force signal to accommodate the change of surface height during tool scan. This capability will greatly enhance the automation and efficiency of the treatment process.

CONCLUSIONS

This study has experimentally investigated the non-resonant piezo vibration striking surface treatment (PVST) process with an emphasis on the striking force, vibration displacement, resulting surface deformation, and their relationships. From this study, the following can be concluded:

1. It is feasible to implement PVST using a piezo stack actuated vibration device installed on a CNC machine platform. PVST can induce strikes with consistent intensity in each cycle of tool vibration. Both the striking intensity and striking location can be well controlled leading to improved control of surface plastic deformation induced by the treatment.
2. In PVST, the tool vibration amplitude during striking is always reduced from the amplitude without striking. This reduction in vibration amplitude is due to the elastic deformation of the vibration device assembly and is linearly dependent on the striking force. The linear force – amplitude reduction relationship reflects the stiffness of the device assembly.
3. In PVST, the depth of the permanent indentation resulting from each strike is, to a first approximation, linearly dependent on the striking peak force. This linear force

relationship offers the opportunity to directly monitor and control the surface deformation induced by each strike using the force signal.

4. The texture and roughness of the treated surface are primarily affected by the striking overlap ratio and tool vibration amplitude in PVST. The finish of the treated surface can be improved by increasing the striking overlap ratio and / or decreasing the vibration amplitude.

The present study has demonstrated the promising capability of PVST in inducing controllable surface deformation. Future studies will focus on how to utilize this capability to realize deformation-based engineering of surface attributes for enhancing components' performance such as wear resistance and fatigue life.

ACKNOWLEDGMENT

This work is supported in part by NSF CMMI grants no. 2019320 and 2102015.

NOMENCLATURE

V	Piezo stack driving voltage
V_{pp}	Peak-to-peak driving voltage amplitude
f	Driving voltage frequency or vibration frequency
u	Tool vibration displacement
u^0_{pp}	Peak-to-peak vibration amplitude w/o striking
u_{pp}	Peak-to-peak vibration amplitude w/ striking
u^0_{max}	Maximum vibration displacement w/o striking
u_{max}	Maximum vibration displacement w striking
F_z	Striking force
F_{max}	Striking peak force
F_x	Sliding force
h	Depth of permanent indentation
D	Diameter of permanent indentation
v_s	Speed of horizontal tool scan (or feed) motion
d_p	Spacing between parallel scan lines
d_s	Spacing between two successive strikes
r_o	Striking overlap ratio

REFERENCES

[1] M'Saoubi, R., Outeiro, J. C., Chandrasekaran, H., Dillon, O. W., and Jawahir, I. S., 2008, "A Review of Surface Integrity in Machining and Its Impact on Functional Performance and Life of Machined Products," Int. J. Sustain. Manuf., **1**(1–2), pp. 203–236.

[2] Torres, M. A. S., and Voorwald, H. J. C., 2002, "An Evaluation of Shot Peening, Residual Stress and Stress Relaxation on the Fatigue Life of AISI 4340 Steel," Int. J. Fatigue, **24**(8), pp. 877–886.

[3] Tekeli, S., 2002, "Enhancement of Fatigue Strength of SAE 9245 Steel by Shot Peening," Mater. Lett., **57**(3), pp. 604–608.

[4] Wang, S., Li, Y., Yao, M., and Wang, R., 1998, "Compressive Residual Stress Introduced by Shot Peening," J. Mater. Process. Technol., **73**(1–3), pp. 64–73.

[5] Wang, S., Li, Y., Yao, M., and Wang, R., 1998, "Fatigue Limits of Shot-Peened Metals," J. Mater. Process. Technol., **73**(1–3), pp. 57–63.

[6] Lu, K., and Lu, J., 2004, "Nanostructured Surface Layer on Metallic Materials Induced by Surface Mechanical Attrition Treatment," Mater. Sci. Eng. A, **375**–**377**(1-2 SPEC. ISS.), pp. 38–45.

[7] Roland, T., Retraint, D., Lu, K., and Lu, J., 2006, "Fatigue Life Improvement through Surface Nanostructuring of Stainless Steel by Means of Surface Mechanical Attrition Treatment," Scr. Mater., **54**(11), pp. 1949–1954.

[8] Tao, N. R., Wang, Z. B., Tong, W. P., Sui, M. L., Lu, J., and Lu, K., 2002, "An Investigation of Surface Nanocrystallization Mechanism in Fe Induced by Surface Mechanical Attrition Treatment," Acta Mater., **50**(18), pp. 4603–4616.

[9] Yildirim, H. C., and Marquis, G. B., 2012, "Fatigue Strength Improvement Factors for High Strength Steel Welded Joints Treated by High Frequency Mechanical Impact," Int. J. Fatigue, **44**, pp. 168–176.

[10] Malaki, M., and Ding, H., 2015, "A Review of Ultrasonic Peening Treatment," Mater. Des., **87**, pp. 1072–1086.

[11] Roy, S., Fisher, J. W., and Yen, B. T., 2003, "Fatigue Resistance of Welded Details Enhanced by Ultrasonic Impact Treatment (UIT)," *International Journal of Fatigue*, Elsevier, pp. 1239–1247.

[12] Bleicher, F., Lechner, C., Habersohn, C., Kozeschnik, E., Adjassoho, B., and Kaminski, H., 2012, "Mechanism of Surface Modification Using Machine Hammer Peening Technology," CIRP Ann. - Manuf. Technol., **61**(1), pp. 375–378.

[13] Schulze, V., Bleicher, F., Groche, P., Guo, Y. B., and Pyun, Y. S., 2016, "Surface Modification by Machine Hammer Peening and Burnishing," CIRP Ann. - Manuf. Technol., **65**(2), pp. 809–832.

[14] Cao, X. J., Pyoun, Y. S., and Murakami, R., 2010, “Fatigue Properties of a S45C Steel Subjected to Ultrasonic Nanocrystal Surface Modification,” Appl. Surf. Sci., **256**(21), pp. 6297–6303.

[15] Suh, C. M., Song, G. H., Suh, M. S., and Pyoun, Y. S., 2007, “Fatigue and Mechanical Characteristics of Nano-Structured Tool Steel by Ultrasonic Cold Forging Technology,” Mater. Sci. Eng. A, **443**(1–2), pp. 101–106.

[16] Berglund, J., Liljengren, M., and Rosén, B. G., 2011, “On Finishing of Pressing Die Surfaces Using Machine Hammer Peening,” Int. J. Adv. Manuf. Technol., **52**(1–4), pp. 115–121.

[17] Mannens, R., Trauth, D., Mattfeld, P., and Klocke, F., 2018, “Influence of Impact Force, Impact Angle, and Stroke Length in Machine Hammer Peening on the Surface Integrity of the Stainless Steel X3CrNiMo13-4,” Procedia CIRP, **71**, pp. 166–171.

[18] Amanov, A., Cho, I. S., Pyoun, Y. S., Lee, C. S., and Park, I. G., 2012, “Micro-Dimpled Surface by Ultrasonic Nanocrystal Surface Modification and Its Tribological Effects,” Wear, **286**–**287**, pp. 136–144.

[19] Telljohann, G., and Dannemeyer, S., 2009, “Hifit - Technische Entwicklung Und Anwendung,” Stahlbau, **78**(9), pp. 622–626.

[20] Ernould, C., Schubnell, J., Farajian, M., Maciolek, A., Simunek, D., Leitner, M., and Stoschka, M., 2019, “Application of Different Simulation Approaches to Numerically Optimize High-Frequency Mechanical Impact (HFMI) Post-Treatment Process,” Weld. World, **63**(3), pp. 725–738.

[21] Altintas, Y., 2000, *Manufacturing Automation: Principles of Metal Cutting and Machine Tool Vibrations*, Cambridge University Press.

[22] Guo, Y., Saldana, C., Dale Compton, W., and Chandrasekar, S., 2011, “Controlling Deformation and Microstructure on Machined Surfaces,” Acta Mater., **59**(11).

[23] Guo, Y., Lee, S. E., and Mann, J. B., 2017, “Piezo-Actuated Modulation-Assisted Drilling System with Integrated Force Sensing,” J. Manuf. Sci. Eng. Trans. ASME, **139**(1).

[24] Guo, Y., and Mann, J. B., 2020, “Control of Chip Formation and Improved Chip Ejection in Drilling with Modulation-Assisted Machining,” J. Manuf. Sci. Eng. Trans. ASME, **142**(7).

[25] Guo, Y., Stalbaum, T., Yeung, H., Chandrasekar, S., and Mann, J., 2013, “Modulation-Assisted High Speed Machining of Compacted Graphite Iron (CGI),” *Transactions of the North American Manufacturing Research Institution of SME*.

[26] Tabor, D., 1948, “A Simple Theory of Static and Dynamic Hardness,” Proc. R. Soc. London. Ser. A. Math. Phys. Sci., **192**(1029).

Figure Captions List

Fig. 1 The real picture (a, b) and the schematic illustration (c) of the experimental setup for PVST.

Fig. 2 The sinusoidal driving voltage input (a) and the corresponding tool vibration displacement (b) at no striking condition for different voltage amplitudes at the same frequency (100 Hz). (c) The correlation of tool vibration amplitude with driving voltage amplitude.

Fig. 3 Schematic illustrations of the experiments conducted in the study: (a) tool-surface approaching; (b) single spot vibration striking; (c) 1D scan vibration striking; (d) 2D scan vibration striking.

Fig. 4 The measured striking force (top) and tool vibration displacement (bottom) plotted against the tool vertical position Z in the tool-surface approaching experiment. f = 100 Hz, V_{pp} = 150 V.

Fig. 5 The relation between the striking peak force and the reduction in maximum tool vibration displacement at (a) f = 10 Hz and (b) f = 100 Hz. (c) The relation between force and tool deflection in a static compression test (no tool vibration).

Fig. 6 Measured tool vibration displacement (a) and striking force (b) in the single spot vibration striking experiment at f = 10 Hz and V_{pp} = 150 V. (c) Detailed variations of force and displacement signals within 4 vibration cycles from t = 4 s to 4.4 s.

Fig. 7 Summary of (a) striking peaking force, (b) maximum tool vibration displacement, and (c) the depth of permanent indentation in single spot vibration striking for various vibration conditions.

Fig. 8 (a) Optical photos of the permanent indentations created in single spot vibration striking at various vibration conditions and their section profiles grouped for (b) f = 10 Hz and (c) f = 100 Hz.

Fig. 9 The correlation of striking peak force with (a) the depth and (b) diameter of the permanent indentation in single spot vibration striking.

Fig. 10 (a) Definition of striking overlap ratio. (b) Optical photo and (c) measured topography of the surface grooves created in 1D scan vibration striking at various striking overlap ratios. f = 100 Hz, V_{pp} = 150 V.

Fig. 11 (a) Longitudinal and (b) transverse section profiles of the surface grooves shown in Fig. 10.

Fig. 12 Striking force (F_z) and sliding force (F_x) in 1D scan vibration striking at various overlap ratios: (a) r_o = 0; (b) r_o = 0.25; (c) r_o = 0.5; (d) r_o = 0.75. f = 100 Hz, V_{pp} = 150 V.

Fig. 13 Comparisons of (a) the depth and (b) width of surface grooves resulting from 1D scan vibration at various V_{pp} and r_o. f = 100 Hz.

Fig. 14 The correlation of the striking peak force with (a) the depth and (b) width of the surface groove in 1D scan vibration striking experiment.

Fig. 15 Surface topography resulting from 2D scan vibration striking at different r_o and V_{pp}. f = 100 Hz. Measured area is 1.4 x 1.4 mm.

Fig. 16 Variations of roughness parameters with r_o and V_{pp} for surfaces shown in Fig. 15.

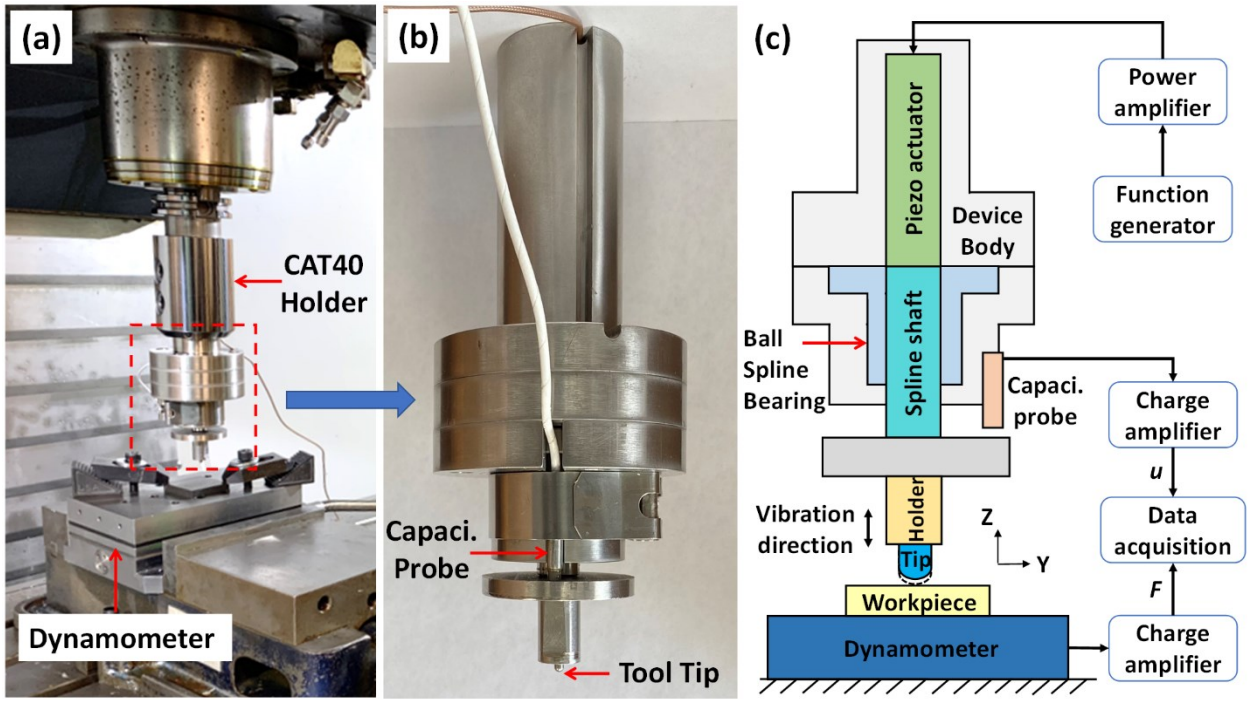

Fig. 1 The real picture (a, b) and the schematic illustration (c) of the experimental setup for PVST.

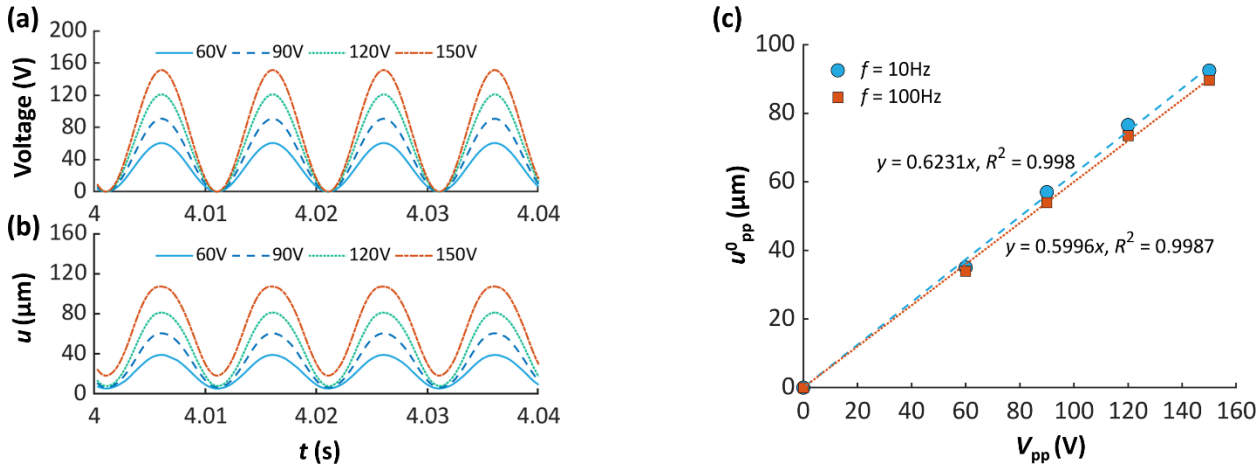

Fig. 2 The sinusoidal driving voltage input (a) and the corresponding tool vibration displacement (b) at no striking condition for different voltage amplitudes at the same frequency (100 Hz). (c) The correlation of tool vibration amplitude with driving voltage amplitude.

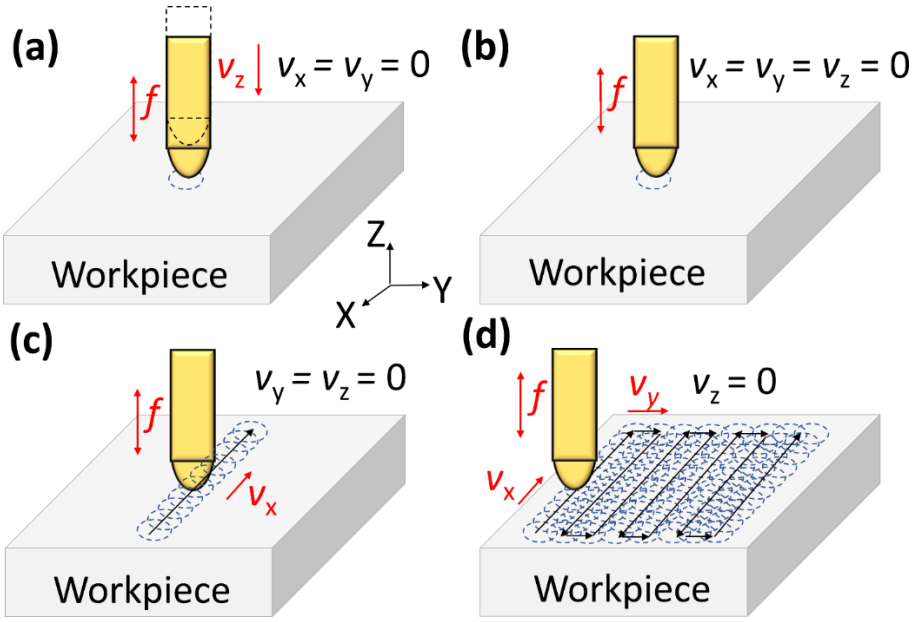

Fig. 3 Schematic illustrations of the experiments conducted in the study: (a) tool-surface approaching; (b) single spot vibration striking; (c) 1D scan vibration striking; (d) 2D scan vibration striking.

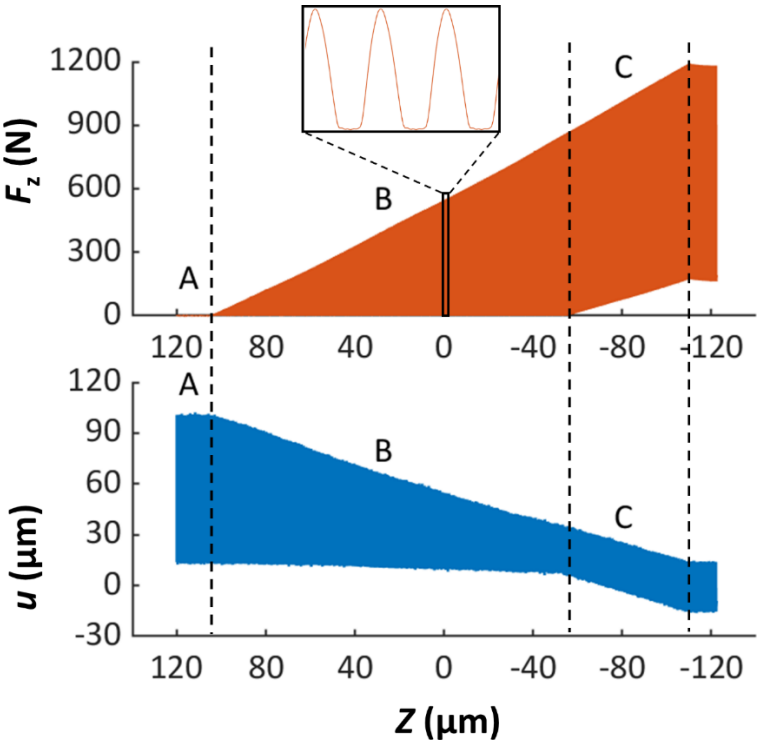

Fig. 4 The measured striking force (top) and tool vibration displacement (bottom) plotted against the tool vertical position Z in the tool-surface approaching experiment. f = 100 Hz, V_{pp} = 150 V.

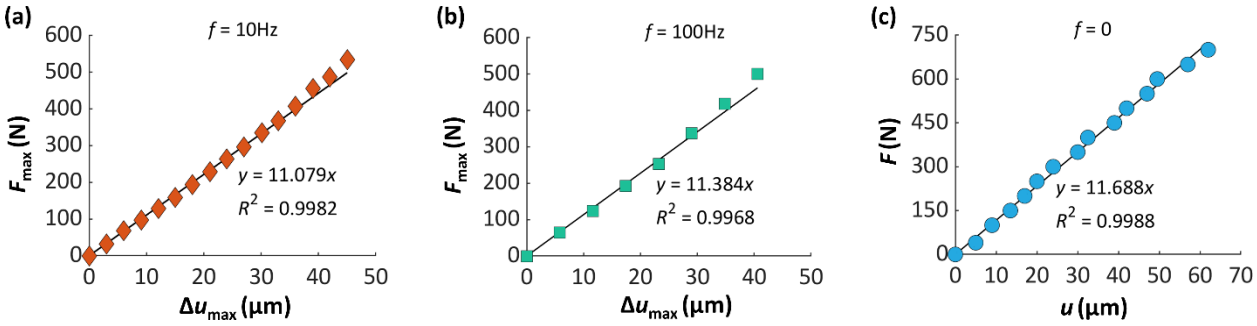

Fig. 5 The relation between the striking peak force and the reduction in maximum tool vibration displacement at (a) f = 10 Hz and (b) f = 100 Hz. (c) The relation between force and tool deflection in a static compression test (no tool vibration).

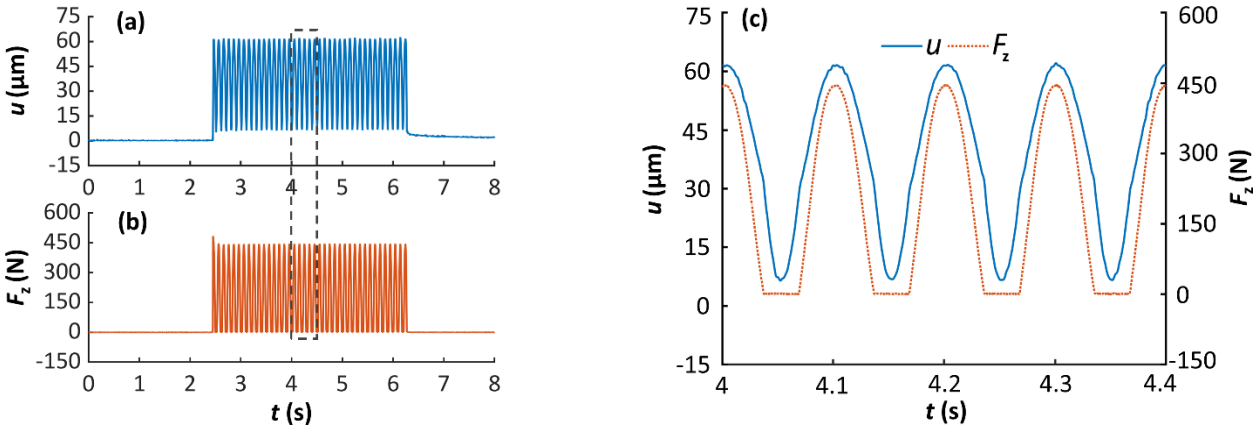

Fig. 6 Measured tool vibration displacement (a) and striking force (b) in the single spot vibration striking experiment at f = 10 Hz and V_{pp} = 150 V. (c) Detailed variations of force and displacement signals within 4 vibration cycles from t = 4 s to 4.4 s.

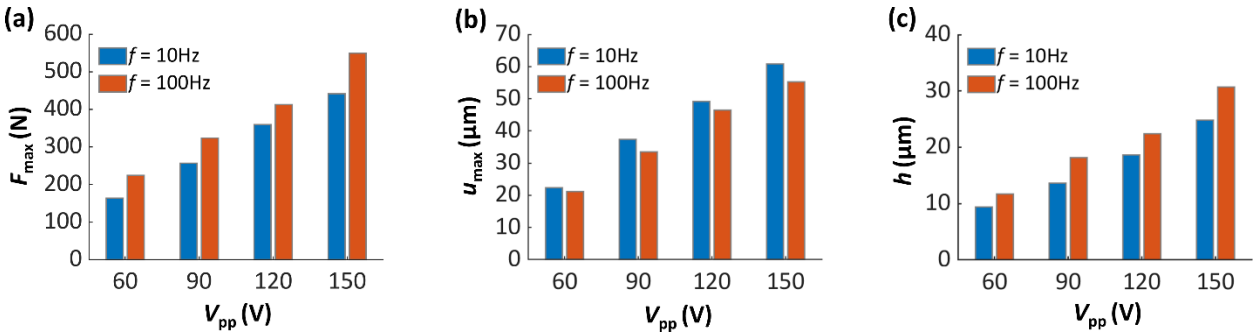

Fig. 7 Summary of (a) striking peaking force, (b) maximum tool vibration displacement, and (c) the depth of permanent indentation in single spot vibration striking for various vibration conditions.

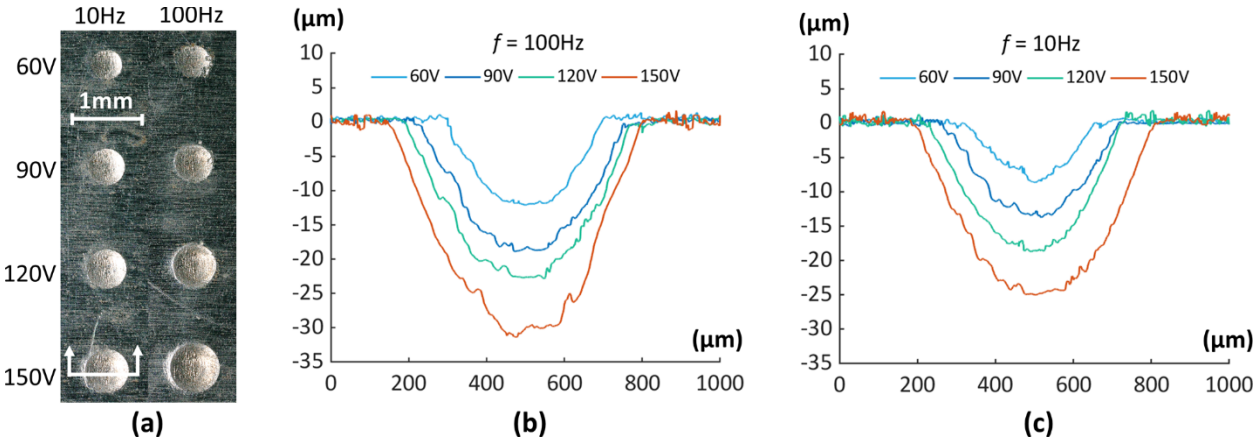

Fig. 8 (a) Optical photos of the permanent indentations created in single spot vibration striking at various vibration conditions and their section profiles grouped for (b) f = 10 Hz and (c) f = 100 Hz.

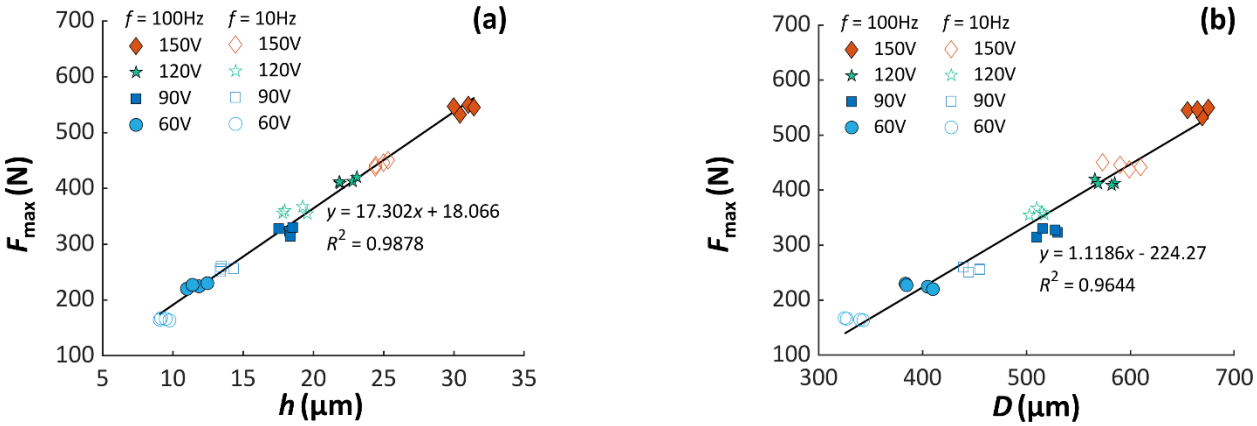

Fig. 9 The correlation of striking peak force with (a) the depth and (b) diameter of the permanent indentation in single spot vibration striking.

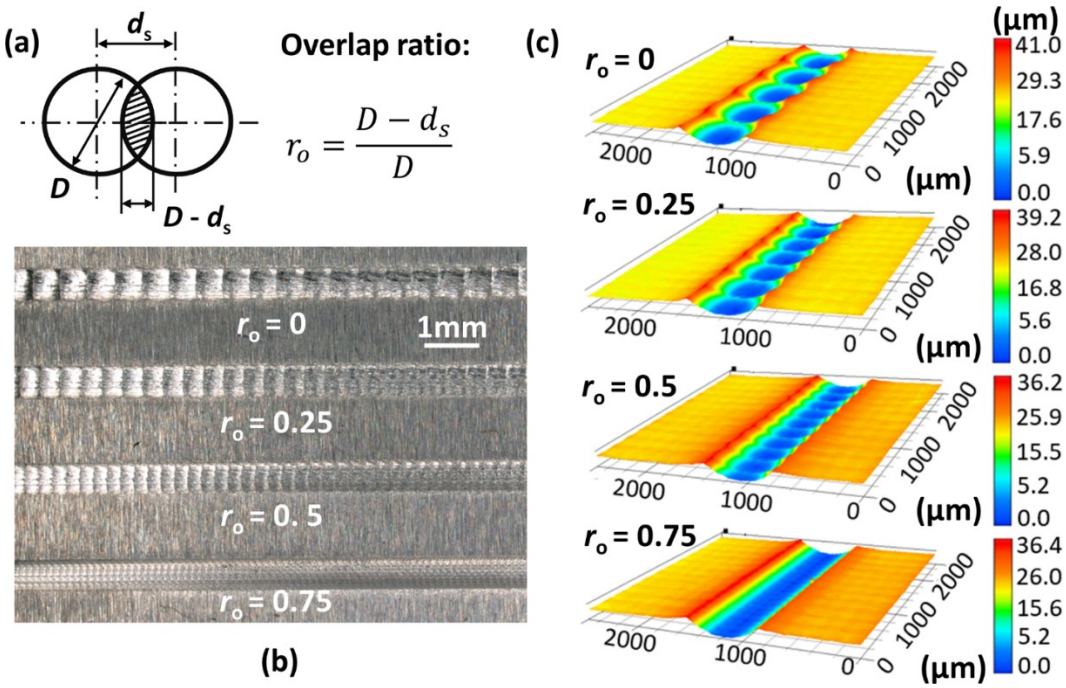

Fig. 10 (a) Definition of striking overlap ratio. (b) Optical photo and (c) measured topography of the surface grooves created in 1D scan vibration striking at various striking overlap ratios. f = 100 Hz, V_{pp} = 150 V.

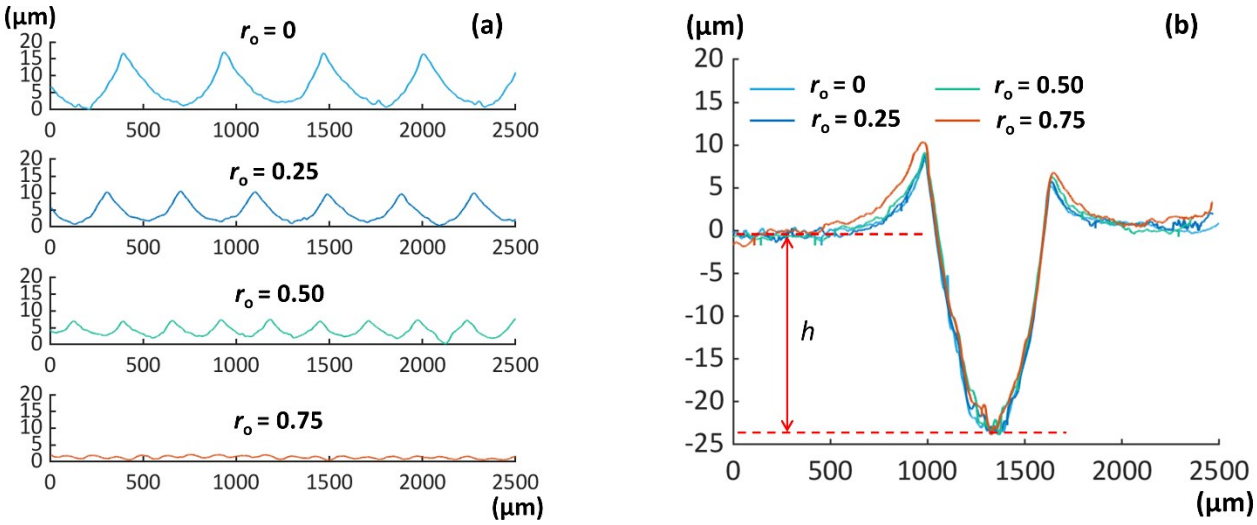

Fig. 11 (a) Longitudinal and (b) transverse section profiles of the surface grooves shown in Fig. 10.

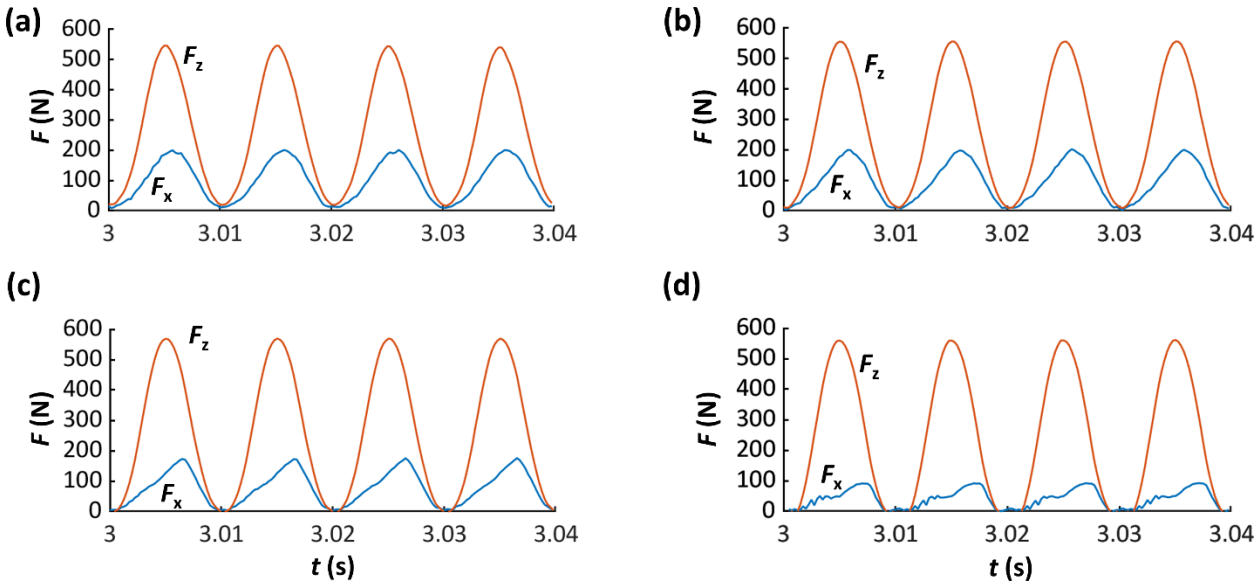

Fig. 12 Striking force (F_z) and sliding force (F_x) in 1D scan vibration striking at various overlap ratios: (a) r_o = 0; (b) r_o = 0.25; (c) r_o = 0.5; (d) r_o = 0.75. f = 100 Hz, V_{pp} = 150 V.

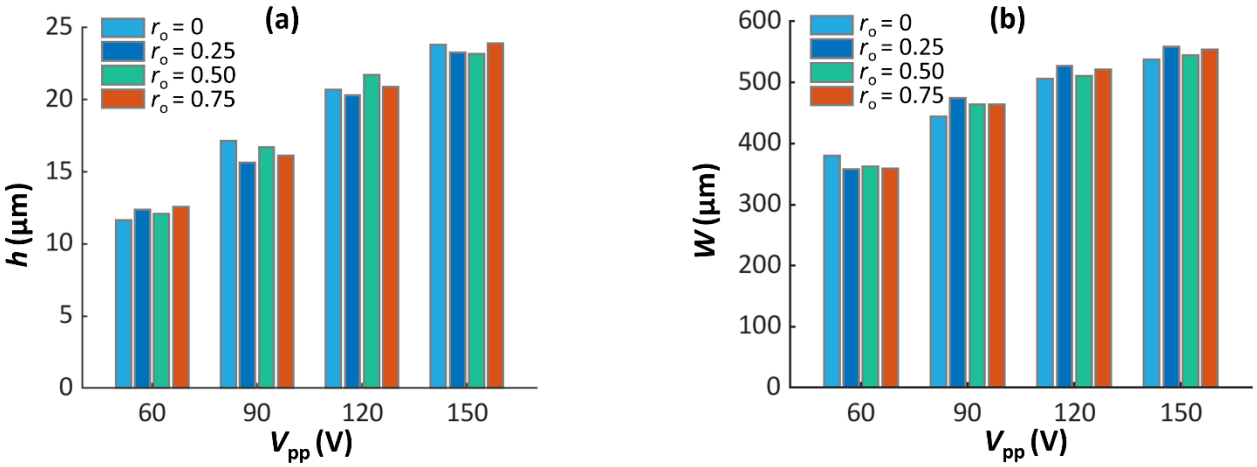

Fig. 13 Comparisons of (a) the depth and (b) width of surface grooves resulting from 1D scan vibration at various V_{pp} and r_o. f = 100 Hz.

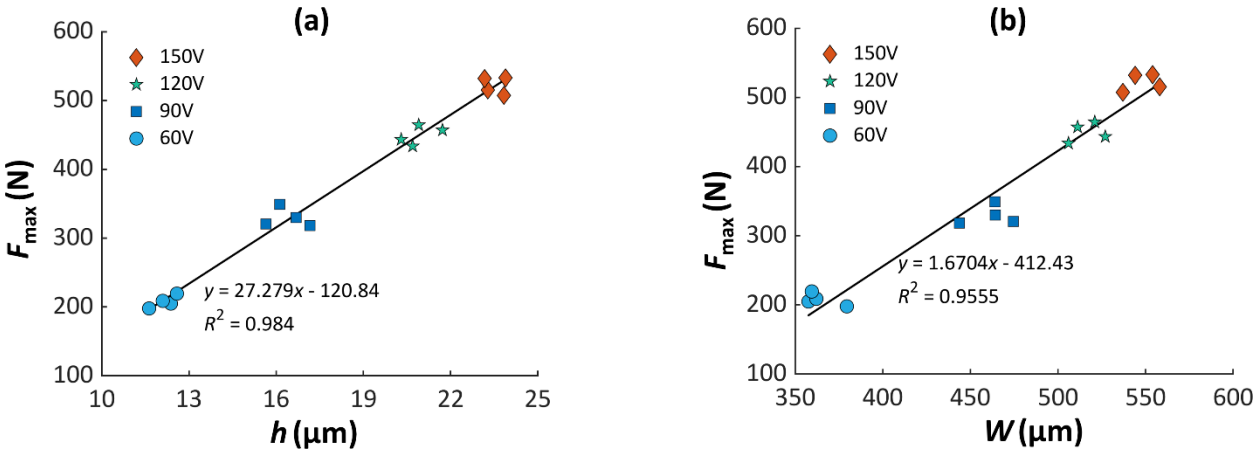

Fig. 14 The correlation of the striking peak force with (a) the depth and (b) width of the surface groove in 1D scan vibration striking experiment.

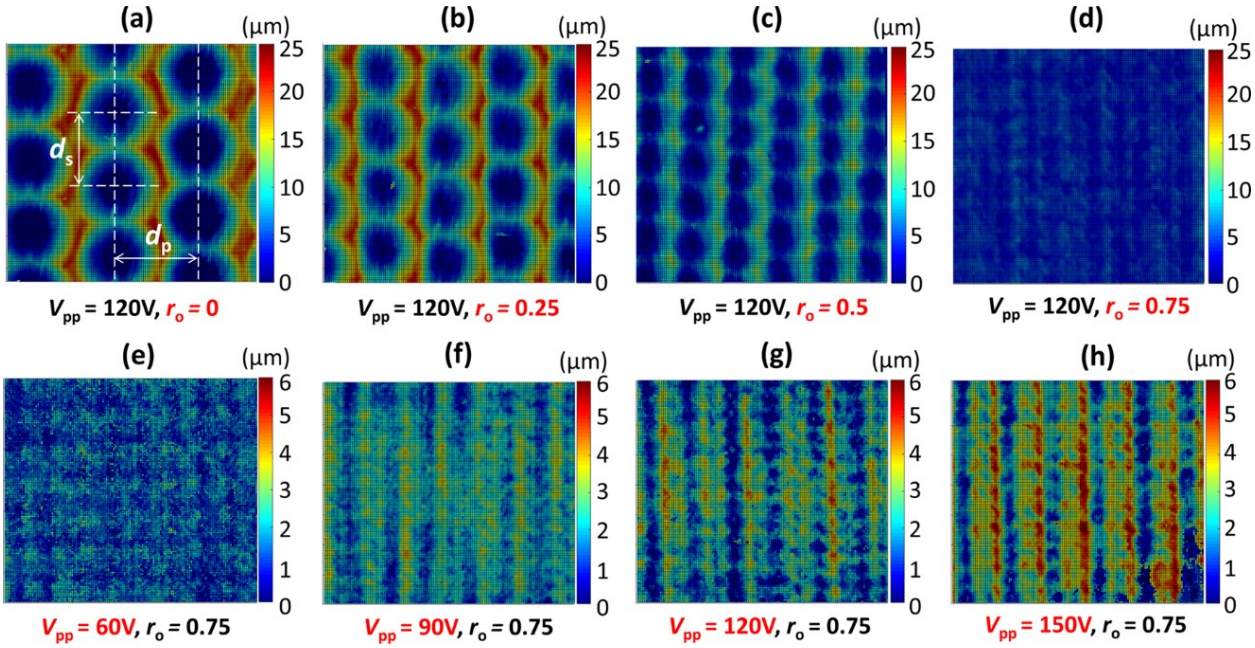

Fig. 15 Surface topography resulting from 2D scan vibration striking at different r_o and V_{pp}. f = 100 Hz. Measured area is 1.4 x 1.4 mm.

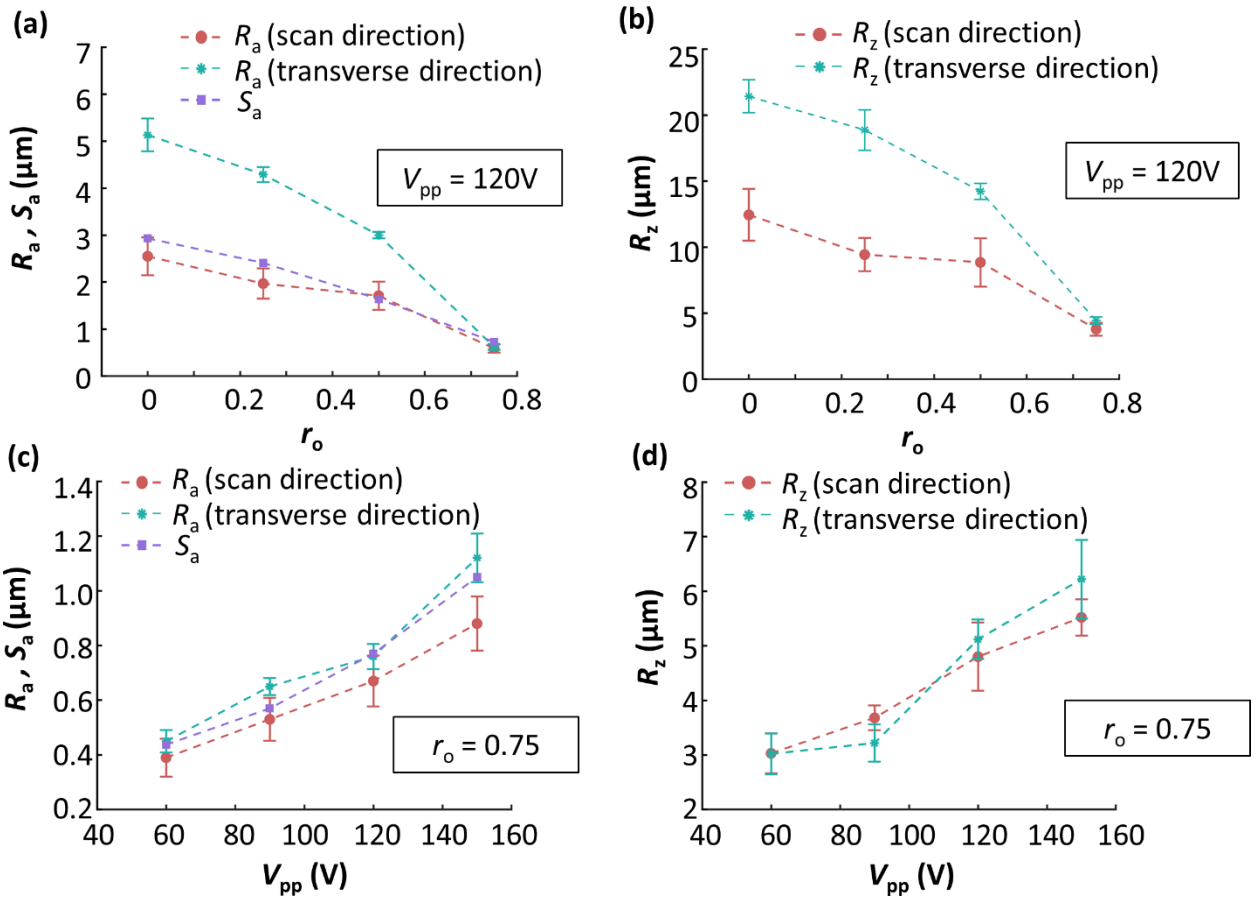

Fig. 16 Variations of roughness parameters with r_o and V_{pp} for surfaces shown in Fig. 15.